Cytoplasmic Abundant Heat-Soluble Proteins from Tardigrades Protect Synthetic Cells Under Stress

Yongkang Xi[a], Jianming Mao[b], Samuel J. Chen[a], Hossein Moghimianavval[a], Young Jin Lee[a], Alexander J. Huang[a], Daniel Zhou[a], Andy Xu[a], Kayla Fu[a], Solomon Adera[a], Andrew L. Ferguson[b,c*], Allen P. Liu[a,d,e,f*]

[a] Department of Mechanical Engineering, University of Michigan, Ann Arbor, MI, 48109 USA

[b] Department of Chemistry, University of Chicago, Chicago, IL, 60637

[c] Pritzker School of Molecular Engineering, University of Chicago, Chicago, IL, 60637

[d] Department of Biomedical Engineering, University of Michigan, Ann Arbor, MI, 48109 USA

[e] Cellular and Molecular Biology Program, University of Michigan, Ann Arbor, MI, 48109 USA

[f] Department of Biophysics, University of Michigan, Ann Arbor, MI, 48109 USA

E-mail:

Andrew L. Ferguson: andrewferguson@uchicago.edu

Allen P. Liu: allenliu@umich.edu

Yongkang Xi and Jianming Mao have equal contributions

Cytoplasmic abundant heat-soluble (CAHS) proteins, a stress-responsive intrinsically disordered protein from tardigrades, have been discovered to form gel-like networks providing structural support during dehydration, thus enabling anhydrobiosis. However, the mechanism by which CAHS proteins protect the dehydrating cellular membrane remains enigmatic. Using giant unilamellar vesicles (GUVs) as a model membrane system, we show that encapsulated CAHS12 undergoes a reversible structural transformation that reinforces membrane integrity and preserves encapsulated components, mimicking natural anhydrobiosis. CAHS12-containing GUVs demonstrated stability for weeks and mechanical robustness under dehydration, elevated temperature, and osmotic stresses. Molecular simulations suggest that CAHS12 forms a filamentous network within the vesicle lumen that mitigates membrane collapse and preserves compartmental architecture. Notably, removal of the N-terminal domain of CAHS12 abrogates this protective function. Synthetic cells with cell-free transcription-translation capabilities survive desiccation and recover biochemical activities, akin to the tun state of the tardigrade. This discovery opens up a protein-based strategy to impart synthetic cells with resilience to desiccation and other environmental stresses, expanding their utility in bioengineering, cold-chain-independent biomanufacturing, and adaptive biointerfaces.

Nature provides compelling examples of organisms that remain viable in near-total absence of water (*1*). Tardigrades exemplify this extreme resilience (*2, 3*). These microscopic invertebrates survive complete desiccation, vacuum, ionizing radiation, and extreme temperatures by entering an ametabolic state known as anhydrobiosis, during which cellular water is expelled, and biological activity is halted indefinitely (*4, 5*). Remarkably, they avoid molecular damage—such as protein denaturation, membrane collapse, and functional impairment—commonly associated with desiccation. While classical models emphasize osmolytes like trehalose or antioxidants (*6*), growing evidence implicates a family of tardigrade intrinsically disordered proteins, namely the cytoplasmic-abundant heat-soluble (CAHS) proteins, as the primary drivers of this exceptional dry-state tolerance (*7*).

Tardigrades possess a diverse repertoire of CAHS proteins with potentially overlapping and isoform-specific functions under stress. CAHS proteins remain unstructured in hydrated conditions but undergo reversible, stress-responsive folding upon drying (*8*), with disordered N and C termini flanking a central α-helical linker domain (**Fig. 1A**). It has been postulated that these heat-soluble proteins protect the membrane via insertion of α-helices to maintain the crystalline state of phospholipids under desiccation (*7*). *In vitro* experiments have demonstrated CAHS proteins' capacity to vitrify (*2*), form hydrogels (*7, 8*), and prevent aggregation under stress (*7, 8*). However, their ability to protect higher-order systems—cells or synthetic assemblies—from dehydration remains largely unexplored (*8*). We chose to study CAHS12, a conserved and abundantly expressed isoform during desiccation, due to its demonstrated capacity to form reversible filamentous networks suitable for reductionist reconstitution in synthetic systems (*8*). Interestingly, we found that expressing a GFP-tagged CAHS12 in *Escherichia coli* enables survival rates exceeding 90% after six days of ambient dry storage, compared to near-total lethality in control strains (**fig. S1**). Though striking, these results cannot resolve molecular mechanisms due to the complexity of cellular environments and overlapping stress responses.

To dissect these mechanisms and engineer programmable desiccation resilience, we turned to giant unilamellar vesicles (GUVs) as a model membrane system and synthetic cells—minimal lipid-bounded compartments that encapsulate functional biochemical systems (*9, 10*). Their simplicity and controllability make them ideal for probing protein-mediated stress protection on membranes. We report a remarkable ability for CAHS proteins to protect synthetic membrane systems against stresses, offering a blueprint for constructing robust, dry-state biotechnologies within synthetic lipid membranes and a putative mechanism for CAHS-mediated dry-state tolerance in living cells.

CAHS12 enables robust structural preservation of synthetic cells during dehydration-rehydration cycles

To determine whether cytoplasmic proteins from tardigrades can confer desiccation tolerance to GUVs, we encapsulated a panel of candidate proteins and subjected them to dehydration–rehydration cycles (**Fig. 1B, fig. S2-S3**). GUVs encapsulating CAHS12-GFP maintained their size after drying and rehydration (8.4 ± 4.1 μm before drying vs. 7.0 ± 2.3 μm after rehydration; n > 100, **fig. S3C**). In contrast, GUVs containing bovine serum albumin (BSA), actin, or no protein underwent aggregation, collapse, or rupture during drying and exhibited only partial recovery. These failures likely reflect membrane stresses arising from steep osmotic gradients and evaporative flux, which compress the bilayer, thin the hydration shell, enhance van der Waals adhesion, and destabilize the air–water interface (*11–13*). Without a stabilizing mechanism, these forces lead to irreversible structural failure and cargo leakage (*e.g.*, Cy5) upon rehydration.

To identify the structural determinants of CAHS12-mediated protection, we generated fluorescent fusion proteins and truncation variants removing either the C or N terminus, hereafter referred to as ΔC and ΔN (**fig. S2 and S13**, **Tables S1, S4, S5**). GUVs encapsulating full-length CAHS12, -GFP or -BFP retained spherical morphology even at 20 μM, indicating that the bulky fluorescent tags do not impair function (**Fig. 1B**, **fig. S4-S5 and S6A**). Likewise, the ΔC variant preserved vesicle shape, suggesting the C-terminal domain is unnecessary (**fig. S6B**). By contrast, the ΔN variant failed to prevent GUV collapse or cargo leakage, even at 280 μM, indicating a critical role for the N-terminal intrinsically disordered regions in protective function (**fig. S6C**). To investigate how CAHS12 preserves vesicle architecture, we imaged dried GUVs using confocal and scanning electron microscopy. Three-dimensional reconstructions showed that GUVs containing 280 μM CAHS12-GFP formed compact but intact spherical structures, with continuous membranes labeled by rhodamine-PE lipids (**Fig. 1C**). GFP fluorescence was evenly distributed across both the membrane and inside. Scanning electron microscopy confirmed smooth, rounded vesicle morphology (**Fig. 1D**), consistent with resistance to interfacial compression and membrane rupture. To probe concentration dependence, we compared CAHS12-GFP at 280, 20, and 10 μM. At high concentration (i.e., 280 μM), CAHS12-GFP appeared uniform (**Fig. 1E, 1F**). At lower concentrations, CAHS12-GFP was distributed to the membrane interface, consistent with cooperative membrane binding via multivalent interactions or weak amphiphilic motifs within the disordered regions (**Fig. 1F, 1G**). Real-time imaging during rehydration revealed rapid morphological recovery (**Fig. 1G**). GUVs with 20 μM CAHS12-GFP expanded within 1 s of water addition and regained spherical geometry by 8 s, while GFP signal

redistributed from uneven to uniform across the membrane, reflecting dynamic re-equilibration with decreasing membrane tension. Similar results were observed during the rehydration of GUVs containing 10 μM CAHS12-GFP (**fig. S7**). These observations suggest that CAHS12-GFP forms a reversible, stress-responsive network that enables compression tolerance and prevents membrane rupture and content loss during desiccation–rehydration transitions.

To understand the physical basis for this protection, we assessed CAHS12's interfacial properties using pendant drop tensiometry (*14*). In the presence of POPC (0.41 mM), CAHS12 lowered interfacial tension (IFT) from ~26 to ~12 mN/m at 0.1 mM, indicative of surface adsorption and tension buffering (**Fig. 1H**) (*15, 16*). To further quantify this interfacial adsorption behavior, we estimated the apparent surface excess concentration (Γ) using the Gibbs adsorption equation, $\Gamma = -(\frac{1}{RT})(\frac{d\gamma}{dln\ c})$, where Γ is the surface excess concentration (mol/m^2), γ is the interfacial tension (N/m), c is the bulk protein concentration (mol/L), R is the universal gas constant (8.314 J·mol^{-1}·K^{-1}), and T is the absolute temperature (K). Over the concentration range of 0.1–1.0 mM, CAHS12 exhibited a modest increase in interfacial tension (from ~12 to ~15 mN/m), corresponding to a surface excess of approximately 5.3×10^{-7} mol/m^2. In contrast, the ΔN variant showed a more pronounced increase in IFT over the same range (from ~6 to ~8 mN/m), yielding a larger estimated surface excess of 1.4×10^{-6} mol/m^2. These results suggest that while the ΔN construct accumulates more extensively at the interface, it may not form a cohesive or stress-buffering network—consistent with its inability to protect vesicle morphology or prevent cargo leakage upon rehydration. This disparity between adsorption quantity and protective efficacy implies that interfacial coverage alone is insufficient; rather, the structural organization and molecular interactions facilitated by the N-terminal domain are likely critical for forming a functional interfacial scaffold. The non-monotonic behavior of CAHS12 (i.e., IFT increasing at higher concentrations) further hints at possible crowding or structural rearrangements at saturated interfaces, which may reflect dynamic assembly processes unique to the full-length protein. At 1 mM, IFT increased slightly (~15 mN/m), possibly due to interfacial saturation or crowding (**Fig. 1I**) (*17*). Both CAHS12-GFP and ΔC variants retained this activity, while ΔN constructs showed minimal IFT reduction (<10 mN/m), confirming the N-terminal region mediates lipid-specific surface interaction. In the absence of POPC, all constructs showed similarly IFT (~20–28 mN/m), indicating that although CAHS12 possesses surface activity, it preferentially interacts with lipid interfaces to regulate interfacial tension (**fig. S8**). We next investigated whether these interfacial properties underlie membrane stabilization. Circularity analysis of dried GUVs showed that full-length and CAHS12 ΔC maintained shape integrity (circularity > 0.85), whereas the ΔN variant yielded deformed

vesicles (circularity < 0.4), consistent with structural failure (**Fig. 1J** and **fig. S9**). Taken together, these results demonstrate that CAHS12 operates as a lipid-specific, disordered interfacial modulator that assembles reversibly at stressed membranes, buffers tension, and enables rapid vesicle recovery following rehydration.

Molecular dynamics simulations of CAHS12 protein assemblies reveal key interactions with phospholipid membranes

To probe the underlying mechanism by which CAHS12 protects GUVs during dehydration, we employed coarse-grained molecular dynamics (MD) simulations using the Martini3 force field (*18*) to model the protein dynamics, assembly behaviors, and interaction with a POPC lipid membrane (**Fig. 2A).** Inspired by prior studies (*19–21*), the CAHS12 protein was modeled as a dumbbell-like construct where the N-terminal (residues 1-153) and C-terminal regions (residues 268-297) were represented as random coils and the linker region (residues 154-267) as an extended α-helix. This structural representation is supported by an analysis of the κ value as a measure of charge patterning within a protein sequence, with high values indicative of disordered conformations (*22*): high local κ values in the terminal regions suggest disordered conformations, and low κ values in the linker region suggest ordered conformations. These secondary structure assignations result in a molecular model of a single CAHS12 protein in water possessing a radius of gyration (R_g) of (5.21 ± 0.11) nm, which falls in a similar regime for other tardigrade disordered proteins (**fig. S10**) (*19, 21*). Using this model, we first explored inter-protein interactions by simulating systems of two CAHS12 molecules. Principal components analysis (PCA) (*23*) of the resulting dimer conformations reveals that CAHS12 dimers associate primarily through interactions of the C- and N-terminal regions (**Fig. 2B** and **fig. S11**). Notably, the N-terminal region mediates stronger binding with interaction energy (IE) averaging ~(-280) kcal/mol, compared to ~(-69) kcal/mol for C-terminal-only interactions, as measured by the short-range inter-protein interaction energy. In simulations of CAHS12 proteins at varying concentrations, protein assembly mediated by the N- and C-terminal regions exhibited a concentration-dependent trend, with higher concentrations leading to increased terminal close contacts per protein (**fig. S12**), which has also been observed in experiments (*24*).

To further dissect the roles of each terminal region in CAHS12 assemblies, we constructed ΔC and ΔN variants by truncating the respective regions while preserving the conformation of the remaining protein (**fig. S13, Tables S1, S4, S5**). Network analyses of multimer simulations with POPC membranes shows that both the wild-type CAHS12 and the ΔC variant form protein

networks and filaments (**Fig. 2C** and **fig. S14**) with comparable cluster numbers, sizes, and node connectivity (**Fig. 2D**). In contrast, the ΔN variant exhibits a significantly reduced capacity to form networks (**Fig. 2C** and **fig. S14**), with increased cluster numbers and decreased cluster sizes and connectivity (**Fig. 2D**). These results highlight the critical role of the N-terminal region as a "sticky" end that promotes aggregation and filament formation, potentially serving as mechanical support for membrane architectures during dehydration, and providing a putative rationale for the experimentally observed role for the N-terminus in conferring protective function (**Fig. 1B**, **fig. S6**). In addition to mediating protein-protein interactions, we hypothesized that the CAHS12 protein may also mediate protein-lipid interactions, anchoring or stabilizing membrane structures under desiccation. Such an idea has been speculated for tardigrade disordered proteins by Hesgrove *et al.* (*7*). To test this, we analyzed contact frequencies between different regions of CAHS12 and the lipid membrane using simulations of the protein network in the presence of a POPC bilayer. Residues, such as serine, threonine, and glycine, in both the N- and C-terminal regions are frequently localized to or embedded within the lipid surface, whereas the linker region showed markedly fewer membrane contacts (**Fig. 2E and fig. S15A**). Trajectory analysis revealed three distinct protein–membrane interaction modes, involving membrane association mediated by the N- and C-terminal regions and the proximity of the α-helix linker to the membrane (**Fig. S16**), suggesting a variety of mechanisms by which CAHS12 engages with lipid structures.

We next simulated dehydration by sequential deletion of water beads in simulations involving CAHS12, CAHS12 ΔN, and CAHS12 ΔC variants in the presence of a POPC membrane. Interestingly, while the CAHS12 ΔC variant exhibited 2-fold higher membrane contacts in the hydrated state (**fig. S15B**), contact frequencies of the CAHS12 ΔC variant and full-length CAHS12 increase to a comparable level under dehydrated conditions (**fig. S17)**. In contrast, the CAHS12 ΔN variant displays a markedly reduced ability to interact with the membrane, further emphasizing the critical role of the N-terminal region in membrane association (**Fig. 2F**, **fig. S17**). These simulation results are in good alignment with experimental findings that both full-length CAHS12 and the ΔC variant protect GUV morphology during dehydration, whereas the ΔN variant fails to do so (**Fig. 1B**, **fig. S6**). Visualization of simulation trajectories further confirms that CAHS12 aggregates and attaches to the membrane surface, which is consistent with experimental observations of a proteinaceous layer forming on membranes during dehydration (**Fig. 1G**). Collectively, these results elucidate a dual role for the CAHS12 protein, particularly its N-terminal region, in driving both protein network formation and membrane association, thereby providing mechanistic insight into how CAHS12 may contribute to membrane stabilization during desiccation.

CAHS12 preserves GUV integrity during long-term storage and under environmental stress

To assess whether CAHS12 can confer long-term membrane stability, we monitored GUV morphology following ambient storage under both hydrated and desiccated conditions. GUVs encapsulating CAHS12-GFP retained their size and spherical shape after 5 to 14 days at room temperature ($p > 0.05$, $n > 100$). Even after 30 and 74 days, vesicles displayed only a slight size reduction but maintained distinct spherical geometry (**Fig. 3A, fig. S18**). In contrast, GUVs lacking CAHS12 or containing the ΔN variant deformed or disappeared after just 5 days of storage, accompanied by cargo leakage; by 14 days, intact vesicles were no longer detectable or sparse (**Fig. 3A, fig. S18**). These findings indicate that CAHS12 substantially delays the structural deterioration of GUVs, likely through interfacial interactions that buffer mechanical stress from water loss or chemical aging.

We next examined whether CAHS12 could stabilize GUVs under prolonged desiccation, mimicking long-term dry storage. GUVs encapsulating full-length CAHS12, CAHS12-GFP, or ΔC variants retained spherical morphology and high vesicle density after 14 days of dehydration at room temperature, with minimal aggregation or rupture (**Fig. 3B**). Notably, vesicle size did not change significantly between 0.5 and 14 days of desiccation ($p > 0.05$), suggesting that CAHS12 maintains membrane architecture even under continuous drying (**Fig. 3C**). In contrast, GUVs containing ΔN variant showed pronounced collapse and membrane failure. To evaluate the robustness under physical stress, we subjected GUVs to heat and osmotic shock—common environmental stressors that challenge membrane integrity. When exposed to temperature from 25 to 80 °C under ambient humidity, GUVs containing CAHS12-GFP retained spherical morphology and high vesicle abundance across the full range, with survival exceeding 80% (**Fig. 3D-E**). In contrast, ΔN-containing or empty GUVs exhibited structural failure even at moderate temperatures (37 °C), with near-complete loss above 45 °C (**fig. S19**). These results underscore the essential role of the N-terminal region in thermal protection and demonstrate an unusually broad thermal operating window relative to traditional protein-based stabilizers. To test CAHS12's ability to buffer against acute osmotic stress (Infusion by an equal volume of a 1200 mOsm/kg glucose solution), we exposed GUVs to a high-osmolarity solution and imaged their morphology at 5- and 40-minutes post-treatment (**Fig. 3F**). CAHS12-GFP–containing GUVs resisted collapse throughout the exposure, maintaining circular geometry. By contrast, CAHS12 ΔN–containing vesicles rapidly lost structure, showing shrinkage, deformation, and rupture within 5 minutes (**fig. S20**). At 40 minutes, few intact vesicles remained. These findings again support a model in which

CAHS12 assembles into a dynamic, stress-responsive protein coating that preserves membrane shape and elasticity under compression. This membrane-centric mechanism may underlie the exceptional survival capacity of tardigrade cells under desiccation and extreme conditions. Moreover, the ability to preserve vesicle architecture under ambient and dry storage conditions provides a foundation for engineering cold-chain–independent synthetic cells and bioformulations with extended shelf life.

Robust preservation and rehydration-triggered activation of cell-free systems

When a tardigrade experiences water scarcity, it enters a dormant state called a tun, losing up to 97% of its body water (*25*). Encouraged by CAHS12's ability to protect synthetic membranes against a range of environmental stresses, we sought to determine if synthetic cells with CAHS proteins could enter a tun state under desiccation. Synthetic cell construction represents a frontier of biological engineering, with the eventual goal of building a functioning cell 'from scratch' (*26–28*). Our synthetic cells consist of GUVs encapsulating cell-free transcription–translation (TX-TL) machinery based on the PURE (Protein synthesis Using Recombinant Elements) system (*29*) and DNA encoding genes of interest. As illustrated in **Fig. 4A,** we hypothesize that CAHS proteins protect synthetic cells against dehydration to arrest biochemical reactions while retaining membrane structure, and rehydration restores cellular functions. Dehydration halts cell-free expression (CFE) activity by water removal, while CAHS proteins preserve the internal contents in a dormant yet structurally intact configuration. Upon rehydration, the previously inactivated TX-TL processes would be reactivated, initiating *de novo* CFE within the synthetic cells. Notably, encapsulation within synthetic cells provides an additional layer of protection during desiccation by physically separating the reaction components from external degradation factors such as proteases and RNases, an advantage not afforded by dehydrating reactions in bulk solution or on paper. Upon rehydration, water re-entry dissolves the CAHS networks, restores molecular mobility, reactivates the previously halted TX-TL machinery, and initiates *de novo* CFE within the synthetic cells. This enables synthetic cells to toggle between dormant and active states while maintaining functional integrity under extreme water loss and environmental stress.

We first assessed whether CAHS12 can preserve enzymatic function through dehydration–rehydration cycles, by encapsulating horseradish peroxidase (HRP) in GUVs and subjecting the system to drying for 12 hours. Upon rehydration, HRP was activated by the addition of hydrogen peroxide, initiating a catalytic reaction. The appearance of the fluorescent product resorufin within the GUVs confirmed that enzymatic activity was retained after desiccation (**fig. S21**), indicating

that CAHS12 enables functional preservation of encapsulated proteins under extreme drying stress.

It has been previously demonstrated that CFE reactions can be freeze-dried onto paper or in a tube to enable diagnostic applications or on-demand biomanufacturing by simply adding water and DNA (*30*, *31*). However, synthetic cells are not expected to survive dehydration without protection, similar to our test in *E. coli* (**fig. S1**). To explore whether CAHS proteins can protect synthetic cells from desiccation stress, we encapsulated CFE components and mCherry-expressing DNA (as a fluorescent reporter) and then evaluated how dry storage duration affects CFE output (**Fig. 4B**). Synthetic cells containing CAHS12-GFP were dehydrated and stored at room temperature for defined time intervals, then rehydrated and incubated at 37 °C to initiate protein expression. After dehydration and rehydration immediately (0 h) to activate TX-TL, we observed strong mCherry fluorescence across nearly all vesicles, confirming efficient preservation of transcriptional and translational activity. After 12 hours of dry storage, synthetic cells maintained structural integrity and expressed mCherry at comparable levels. Even after 5 days of storage, rehydrated GUVs maintained high expression levels, demonstrating sustained biochemical activity. Remarkably, after 40 days or even 60 days of ambient storage, GUVs still preserved morphology and measurable CFE activity, though expression levels became heterogeneous. In contrast, and as expected, synthetic cells lacking CAHS12-GFP did not activate CFE upon rehydration (**fig. S22**). These findings indicate a gradual decline in system performance over time but highlight the surprising durability of both lipid membranes and encapsulated TX-TL machinery under non-refrigerated, dry storage conditions.

The successful rebooting of CFE in synthetic cells following prolonged desiccation prompted us to ask whether other synthetic cell functions can be preserved. We are particularly interested in membrane-active properties, as most cell-cell communication takes place at the membrane interface via membrane proteins. As a proof-of-concept demonstration, we synthesized the bacterial mechanosensitive channel (*32–34*), MscL, *de novo* via CFE inside synthetic cells under different conditions, which can be subsequently activated by membrane tension to mediate cargo release. The working model (**Fig. 4C**) depicts MscL as a pentameric transmembrane pore that responds to hypotonic stress by sensing membrane tension (*35*). Upon rehydration and followed by hypo-osmotic induction, water influx generates lateral tension across the synthetic cell membrane, triggering MscL opening and rapid efflux of encapsulated cargo. To test this, desiccation-resistant synthetic cells co-encapsulating a fluorescent cargo (i.e., Cy5) and membrane label (i.e., Rhod-PE) underwent CFE expressing MscL, followed by dehydration–rehydration to test MscL functionality. In hypertonic conditions, Cy5 remained well-encapsulated,

as expected (**Fig. 4D** and **fig. S23**). Under hypotonic stress, Cy5 fluorescence rapidly dissipated from the vesicle interior (**Fig. 4E** and **fig. S23**), with increased background signal and flattening of radial gradients, indicating leakage. Rhod-PE signal confirmed that the membrane was preserved while permeability was altered. These results support successful membrane integration and mechanical gating of MscL to trigger cargo release.

To dissect the sequence of events required for successful MscL-mediated release, we compared desiccation-resistant synthetic cells with or without MscL-encoding DNA after CFE, dehydration–rehydration, and hypotonic challenge (**Fig. 4F**). In freshly prepared synthetic cells, both conditions retained Cy5 cargo. After dehydration for 12 hours and rehydration, synthetic cell morphology and content remained intact. Rehydration in the presence of CFE reagents resulted in pronounced Cy5 loss following hypotonic exposure only in synthetic cells containing MscL DNA, confirming that membrane tension alone was insufficient to induce leakage in the absence of MscL. These findings demonstrate that synthetic cells can be used as long-lived, rehydration-activated chassis for synthetic gene expression and functional protein integration.

To determine whether CAHS12 preserves membrane protein function following dehydration and rehydration, we tested a model of membrane-mediated communication between synthetic and living cells using a juxtacrine signaling system based on SpyTag/SpyCatcher conjugation (*36*). In this platform, HEK293T cells stably express a membrane-anchored SpyCatcher fused to one half of split superfolder Cherry (sfCherry1–10), hereafter referred to as InterCatch, served as the living cell component. Synthetic cells were functionalized with SpyTag fused to a blue fluorescent protein and the C-terminal sfCherry fragment (sfCherry11) to form a SpyTag–BFP–sfCherry11 fusion. This fusion was anchored to the synthetic membrane via Ni^{2+}–His_6 coordination to surface-displayed lipids containing nickel–nitrilotriacetic acid (Ni–NTA).

As a validation step, we first confirmed successful sfCherry complementation in solution using purified SpyTag–BFP–sfCherry11 and InterCatch proteins, which yielded robust red fluorescence upon coincubation, indicating functional interaction between the split fragments (**Fig. 4H** and **fig. 24A-B**). sfCherry complementation is also preserved in HEK293T cells expressing InterCatch-GFP incubated with soluble SpyTag-BFP (**Fig. 4I**). We then tested whether synthetic cells could support this interaction following stress. SpyTag–BFP–functionalized synthetic cells (contained 100 μM CAHS12) dehydrated under vacuum conditions (12 h at 25 °C), and subsequently rehydrated in PBS. Rehydrated synthetic cells were applied to a monolayer of adherent HEK293T–InterCatch cells and incubated at 37 °C for 4 hours. Fluorescence microscopy revealed red sfCherry signal localized at the interface between synthetic and living cells, consistent with membrane-proximal complementation of the split protein (**Fig. 4J** and **fig. S24C**).

Control experiments confirmed that the interaction was specific and dependent on both the membrane display of SpyTag and the presence of CAHS12 (**Fig. 4J**). No sfCherry fluorescence was observed when synthetic cells lacking SpyTag–BFP were applied to InterCatch cells, regardless of dehydration state. Similarly, dehydrated synthetic cells lacking CAHS12 showed little to no synthetic cell formation upon rehydration, and no sfCherry signal was observed after incubation with InterCatch cells, underscoring CAHS's ability to preserve membrane protein display and functional architecture under desiccation stress. Our results reveal that the tardigrade-derived protein CAHS12 acts as a membrane-active, intrinsically disordered polymer that preserves synthetic cell architecture under extreme physical stress. Through its N-terminal region, CAHS12 engages lipid interfaces, forming a dynamic, reversible coating that buffers dehydration-induced membrane stress, prevents rupture, and enables rapid structural recovery upon rehydration. Structural, biophysical, and computational analyses converge on a mechanism wherein CAHS12 stabilizes vesicle shape and integrity by modulating interfacial energetics and assembling into stress-responsive supramolecular networks.

The global biotechnology sector remains tethered to cold-chain logistics (*37–39*). From mRNA vaccines to engineered microbes, nearly all bioactive materials require refrigeration or freezing to maintain efficacy during storage and transport (*40*). This dependence limits deployment in remote or resource-constrained regions. The protective function by CAHS proteins extends to cell-free gene expression systems: dehydrated CAHS12-stabilized synthetic cells retain biosynthetic capacity after long-term ambient storage and are reactivated by simple rehydration. Reconstituted mechanosensitive channels further enable stimulus-triggered molecular release, mimicking biological secretory functions. These findings establish a modular platform for engineering desiccation-tolerant synthetic cells with programmable behaviors, opening new avenues for field-deployable biosystems, cold-chain–independent biomanufacturing, and adaptive biointerfaces.

Acknowledgements

We thank Takekazu Kunieda (University of Tokyo) for sharing the CAHS12 plasmid. We thank Alexandre Bisson (Brandeis University) and the Liu lab for helpful discussion. **Funding:** Research was sponsored by the Army Research Office and was accomplished under Award Numbers: W911NF-23-1-0050 and W911NF-23-1-0084. The views and conclusions contained in this document are those of the authors and should not be interpreted as representing the official policies, either expressed or implied, of the Army Research Office or the U.S. Government. The U.S. Government is authorized to reproduce and distribute reprints for Government purposes notwithstanding any copyright notation herein. This work was completed in part with resources

provided by the University of Chicago Research Computing Center. We gratefully acknowledge computing time on the University of Chicago high-performance GPU-based cyberinfrastructure supported by the National Science Foundation under Grant No. DMR-1828629. This work used Delta GPU compute at NCSA UIUC through allocation CHE240166 from the Advanced Cyberinfrastructure Coordination Ecosystem: Services & Support (ACCESS) program (*41*), which is supported by U.S. National Science Foundation grants #2138259, #2138286, #2138307, #2137603, and #2138296. **Author contributions:** Conceptualization: Y.X., A.P.L. Methodology: Y.X., J.M., H.M., A.L.F., A.P.L. Investigation: Y.X., J.M., S.J.C., Y.J.L., A.J.H., D.Z., A.X. K.F.. Funding acquisition: A.L.F., A.P.L. Writing – original draft: Y.X., J.M., S.J.C., Y.J.L., A.L.F., A.P.L. Writing – review & editing: Y.X., J.M., S.J.C., H.M., Y.J.L., A.J.H., D.Z., A.X., K.F., S.A., A.L.F., A.P.L.. **Competing Interests:** A.L.F. is a co-founder and consultant of Evozyne, Inc. and a co-author of US Patent Applications 16/887,710 and 17/642,582, US Provisional Patent Applications 62/853,919, 62/900,420, 63/314,898, 63/479,378, 63/521,617, and 63/669,836, and International Patent Applications PCT/US2020/035206, PCT/US2020/050466, and PCT/US24/10805. **Data and materials availability:** Gromacs scripts for conducting coarse-grained molecular dynamics simulations of CAHS12 proteins and their interactions with a POPC lipid membrane, along with Jupyter notebooks for analyzing the simulation trajectories and generating plots, are available at https://github.com/Ferg-Lab/CAHS-Protein-Simulations.git. Experimental data are available upon request.

Reference

1. J. H. Crowe, F. A. Hoekstra, L. M. Crowe, Anhydrobiosis. *Annu. Rev. Physiol.* **54**, 579–599 (1992).

2. T. C. Boothby, H. Tapia, A. H. Brozena, S. Piszkiewicz, A. E. Smith, I. Giovannini, L. Rebecchi, G. J. Pielak, D. Koshland, B. Goldstein, Tardigrades Use Intrinsically Disordered Proteins to Survive Desiccation. *Mol. Cell* **65**, 975-984.e5 (2017).

3. N. Møbjerg, K. A. Halberg, A. Jørgensen, D. Persson, M. Bjørn, H. Ramløv, R. M. Kristensen, Survival in extreme environments - on the current knowledge of adaptations in tardigrades. *Acta Physiol.* **202**, 409–420 (2011).

4. J. C. Wright, Cryptobiosis 300 Years on from van Leuwenhoek: What Have We Learned about Tardigrades? *Zool. Anz.* **240**, 563–582 (2001).

5. D. Persson, K. A. Halberg, A. Jørgensen, C. Ricci, N. Møbjerg, R. M. Kristensen, Extreme stress tolerance in tardigrades: surviving space conditions in low earth orbitTardigradi nello spazio: sopravvivenza a condizioni estreme. *J. Zool. Syst. Evol. Res.* **49**, 90–97 (2011).

6. J. H. Crowe, Anhydrobiosis: An Unsolved Problem with Applications in Human Welfare. *Subcell. Biochem.* **71**, 263–280 (2015).

7. C. Hesgrove, T. C. Boothby, The biology of tardigrade disordered proteins in extreme stress tolerance. *Cell Commun. Signal.* **18**, 1–15 (2020).

8. A. Tanaka, T. Nakano, K. Watanabe, K. Masuda, G. Honda, S. Kamata, R. Yasui, H. Kozuka-Hata, C. Watanabe, T. Chinen, D. Kitagawa, S. Sawai, M. Oyama, M. Yanagisawa, T. Kunieda, Stress-dependent cell stiffening by tardigrade tolerance proteins that reversibly form a filamentous network and gel. *PLoS Biol.* **20**, e3001780 (2022).

9. K. P. Adamala, D. A. Martin-Alarcon, K. R. Guthrie-Honea, E. S. Boyden, Engineering genetic circuit interactions within and between synthetic minimal cells. *Nat. Chem.* **9**, 431–439 (2017).

10. C. Guindani, L. C. da Silva, S. Cao, T. Ivanov, K. Landfester, Synthetic Cells: From Simple Bio-Inspired Modules to Sophisticated Integrated Systems. *Angew. Chem. Int. Ed.* **61** (2022).

11. M. Potfis, Desiccation tolerance of prokaryotes. *Microbiol. Rev.* **58**, 755–805 (1994).

12. F. A. Hoekstra, E. A. Golovina, J. Buitink, Mechanisms of plant desiccation tolerance. *Trends Plant Sci.* **6**, 431–438 (2001).

13. J. H. Crowe, J. F. Carpenter, L. M. Crowe, The role of vitrification in anhydrobiosis. *Annu. Rev. Physiol.* **60**, 73–103 (1998).

14. Y. Xi, B. Liu, S. Wang, S. Wei, S. Yin, T. Ngai, X. Yang, CO_2 -responsive Pickering emulsions stabilized by soft protein particles for interfacial biocatalysis. *Chem. Sci.* **13**, 2884–2890 (2022).

15. J. Ji, L. Sun, Z. Luo, Y. Zhang, W. Xianzheng, Y. Liao, X. Tong, J. Shan, Potential Therapeutic Applications of Pulmonary Surfactant Lipids in the Host Defence Against Respiratory Viral Infections. *Front. Immunol.* **12**, 730022 (2021).

16. O. H. S. Ollila, A. Lamberg, M. Lehtivaara, A. Koivuniemi, I. Vattulainen, Interfacial Tension and Surface Pressure of High Density Lipoprotein, Low Density Lipoprotein, and Related Lipid Droplets. *Biophys. J.* **103**, 1236–1244 (2012).

17. T. Wang, N. Wang, Y. Dai, D. Yu, J. Cheng, Interfacial adsorption properties, rheological properties and oxidation kinetics of oleogel-in-water emulsion stabilized by hemp seed protein. *Food Hydrocoll.* **137**, 108402 (2023).

18. P. C. T. Souza, R. Alessandri, J. Barnoud, S. Thallmair, I. Faustino, F. Grünewald, I. Patmanidis, H. Abdizadeh, B. M. H. Bruininks, T. A. Wassenaar, P. C. Kroon, J. Melcr, V. Nieto, V. Corradi, H. M. Khan, J. Domański, M. Javanainen, H. Martinez-Seara, N. Reuter, R. B. Best, I. Vattulainen, L. Monticelli, X. Periole, D. P. Tieleman, A. H. de Vries, S. J. Marrink, Martini 3: a general purpose force field for coarse-grained molecular dynamics. *Nat. Methods* **18**, 382–388 (2021).

19. A. Malki, J. M. Teulon, A. R. Camacho-Zarco, S. wen W. Chen, W. Adamski, D. Maurin, N. Salvi, J. L. Pellequer, M. Blackledge, Intrinsically Disordered Tardigrade Proteins Self-Assemble into Fibrous Gels in Response to Environmental Stress. *Angew. Chem. Int. Ed.* **61**, e202109961 (2022).

20. T. Hashimoto, D. D. Horikawa, Y. Saito, H. Kuwahara, H. Kozuka-Hata, T. Shin-I, Y. Minakuchi, K. Ohishi, A. Motoyama, T. Aizu, A. Enomoto, K. Kondo, S. Tanaka, Y. Hara, S. Koshikawa, H. Sagara, T. Miura, S. I. Yokobori, K. Miyagawa, Y. Suzuki, T. Kubo, M. Oyama, Y. Kohara, A. Fujiyama, K. Arakawa, T. Katayama, A. Toyoda, T. Kunieda, Extremotolerant tardigrade genome and improved radiotolerance of human cultured cells by tardigrade-unique protein. *Nat. Commun. 2016 7:1* **7**, 1–14 (2016).

21. S. Sanchez-Martinez, K. Nguyen, S. Biswas, V. Nicholson, A. V. Romanyuk, J. Ramirez, S. Kc, A. Akter, C. Childs, E. K. Meese, E. T. Usher, G. M. Ginell, F. Yu, E. Gollub, M. Malferrari, F. Francia, G. Venturoli, E. W. Martin, F. Caporaletti, G. Giubertoni, S. Woutersen, S. Sukenik, D. N. Woolfson, A. S. Holehouse, T. C. Boothby, Labile assembly of a tardigrade protein induces biostasis. *Protein Sci.* **33**, e4941 (2024).

22. R. K. Das, R. V. Pappu, Conformations of intrinsically disordered proteins are influenced by linear sequence distributions of oppositely charged residues. *Proc. Natl. Acad. Sci. U. S. A.* **110**, 13392–13397 (2013).

23. J. Lever, M. Krzywinski, N. Altman, Points of Significance: Principal component analysis. *Nat Methods* **14**, 641–643 (2017).

24. M. A. Barilla, S. O. Shuster, C. Davis, Tardigrade CAHS hydrogels protect proteins through concentration-dependent mechanism. *Biophys. J.* **123**, 75a–76a (2024).

25. R. O. Schill, Ed., Water Bears: The Biology of Tardigrades. **2** (Springer, 2018).

26. V. Noireaux, A. P. Liu, The New Age of Cell-Free Biology. *Annu. Rev. Biomed. Eng.* **22**, 51–77 (2020).

27. P. Schwille, J. Spatz, K. Landfester, E. Bodenschatz, S. Herminghaus, V. Sourjik, T. J. Erb, P. Bastiaens, R. Lipowsky, A. Hyman, P. Dabrock, J. C. Baret, T. Vidakovic-Koch, P. Bieling, R. Dimova, H. Mutschler, T. Robinson, T. Y. D. Tang, S. Wegner, K. Sundmacher, MaxSynBio: Avenues Towards Creating Cells from the Bottom Up. *Angew. Chem. Int. Ed.* **57**, 13382–13392 (2018).

28. L. J. Rothschild, N. J. H. Averesch, E. A. Strychalski, F. Moser, J. I. Glass, R. Cruz Perez, I. O. Yekinni, B. Rothschild-Mancinelli, G. A. Roberts Kingman, F. Wu, J. Waeterschoot, I. A. Ioannou, M. C. Jewett, A. P. Liu, V. Noireaux, C. Sorenson, K. P. Adamala, Building Synthetic Cells—From the Technology Infrastructure to Cellular Entities. *ACS Synth. Biol.* **13**, 974–997 (2024).

29. Y. Shimizu, A. Inoue, Y. Tomari, T. Suzuki, T. Yokogawa, K. Nishikawa, T. Ueda, Cell-free translation reconstituted with purified components. *Nat. Biotechnol.* **19**, 751–755 (2001).

30. K. Pardee, S. Slomovic, P. Q. Nguyen, J. W. Lee, N. Donghia, D. Burrill, T. Ferrante, F. R. McSorley, Y. Furuta, A. Vernet, M. Lewandowski, C. N. Boddy, N. S. Joshi, J. J. Collins, Portable, On-Demand Biomolecular Manufacturing. *Cell* **167**, 248-259.e12 (2016).

31. K. Pardee, A. A. Green, T. Ferrante, D. E. Cameron, A. Daleykeyser, P. Yin, J. J. Collins, Paper-based synthetic gene networks. *Cell* **159**, 940–954 (2014).

32. Z. A. Manzer, S. Ghosh, M. L. Jacobs, S. Krishnan, W. R. Zipfel, M. Pineros, N. P. Kamat, S. Daniel, Cell-Free Synthesis of a Transmembrane Mechanosensitive Channel Protein into a Hybrid-Supported Lipid Bilayer. *ACS Appl. Bio. Mater.* **4**, 3101–3112 (2021).

33. J. Garamella, S. Majumder, A. P. Liu, V. Noireaux, An Adaptive Synthetic Cell Based on Mechanosensing, Biosensing, and Inducible Gene Circuits. *ACS Synth. Biol.* **8**, 1913–1920 (2019).

34. S. Majumder, J. Garamella, Y. L. Wang, M. Denies, V. Noireaux, A. P. Liu, Cell-sized mechanosensitive and biosensing compartment programmed with DNA. *Chem. Commun.* **53**, 7349–7352 (2017).

35. C. D. Cox, N. Bavi, B. Martinac, Bacterial Mechanosensors. *Annu. Rev. Physiol.* **80**, 71–93 (2018).

36. H. Moghimianavval, C. Patel, S. Mohapatra, S. W. Hwang, T. Kayikcioglu, Y. Bashirzadeh, A. P. Liu, T. Ha, Engineering Functional Membrane–Membrane Interfaces by InterSpy. *Small* **19**, 2202104 (2023).

37. J. C. Stark, T. Jaroentomeechai, T. D. Moeller, J. M. Hershewe, K. F. Warfel, B. S. Moricz, A. M. Martini, R. S. Dubner, K. J. Hsu, T. C. Stevenson, B. D. Jones, M. P. DeLisa, M. C. Jewett, On-demand biomanufacturing of protective conjugate vaccines. *Sci. Adv.* **7** (2021).

38. M. Prabhakaran, F. Matassoli, D. Leggat, A. Hoover, A. Srikanth, W. Wu, A. R. Henry, J. Wang, B. C. Lin, I. T. Teng, C. A. Schramm, M. Castro, L. Serebryannyy, N. Jean-Baptiste, C. Moore, S. Gajjala, J. P. M. Todd, E. McCarthy, S. Narpala, J. Francica, K. S. Corbett-Helaire, D. C. Douek, P. D. Kwong, R. A. Seder, S. F. Andrews, A. B. McDermott, Adjuvanted SARS-CoV-2 spike protein vaccination elicits long-lived plasma cells in nonhuman primates. *Sci. Transl. Med.* **16**, 5960 (2024).

39. U. Kartoglu, J. Milstien, Tools and approaches to ensure quality of vaccines throughout the cold chain. *Expert Rev. Vaccines* **13**, 843–854 (2014).

40. M. N. Uddin, M. A. Roni, Challenges of Storage and Stability of mRNA-Based COVID-19 vaccines. *Vaccines* **9**, 1033 (2021).

41. T. J. Boerner, S. Deems, T. R. Furlani, S. L. Knuth, J. Towns, ACCESS: Advancing Innovation: NSF's Advanced Cyberinfrastructure Coordination Ecosystem: Services & Support. *PEARC 2023 - Computing for the common good: Practice and Experience in Advanced Research Computing*, 173–176 (2023).

42. E. C. Meng, T. D. Goddard, E. F. Pettersen, G. S. Couch, Z. J. Pearson, J. H. Morris, T. E. Ferrin, UCSF ChimeraX: Tools for structure building and analysis. *Protein Sci.* **32**, e4792 (2023).

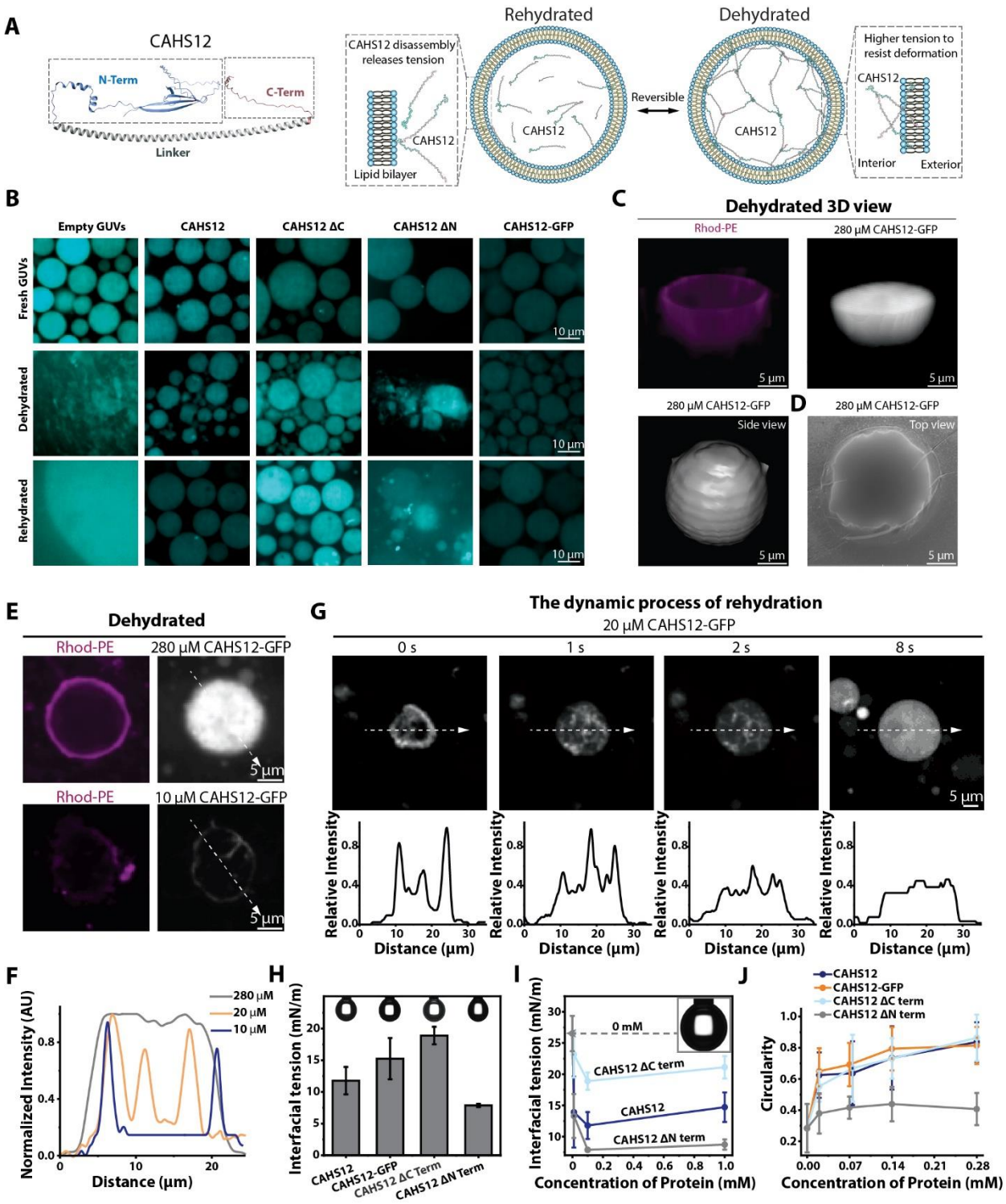

Fig. 1. Structural configuration and functional role of CAHS12 in desiccation-tolerant GUVs. (**A**) Proposed model of CAHS12-mediated stabilization of GUV membranes during dehydration and rehydration. (left) Structural organization of CAHS12, showing an intrinsically disordered N-terminal region (blue), a central α-helical linker (gray), and a disordered C-terminal region (red);

(right) Schematic illustrating CAHS12 behavior during rehydration: CAHS12 disassembles from the membrane interface, releasing tension and allowing fluidity of lipids on the membrane while maintaining structural integrity. Under dehydration, CAHS12 assembles into a reversible, filamentous network across the lipid bilayer interior, increasing interior membrane tension to resist deformation and collapse. This reversible stress-responsive assembly enables membranes to preserve architecture during extreme water loss. Molecular rendering of the CAHS12 protein was constructed using ChimeraX (*42*). (**B**) Fluorescence microscopy of CAHS12-loaded GUVs under fresh, dehydrated, and rehydrated states, where Cy5 encapsulated in GUVs was used to measure the integrity of the GUV membrane structure based on its release; Scale bars, 10 µm. Z-axis scan 3D fluorescence microscopy image (**C**) and scanning electron microscopy image (**D**) of dehydrated GUVs. The magenta signal on the left represents the membrane-localized Rhod-PE, and CAHS12-GFP is shown in gray (right and bottom left); scale bar, 5 µm. (**E**) Fluorescence microscopy image of dehydrated GUVs containing 280 µM or 10 µM of CAHS12-GFP. (**F**) Line scan analysis of normalized GFP fluorescence across dehydrated GUV containing 10, 20, or 280 µM CAHS12-GFP; Scale bar, 5 µm. (**G**) The dynamic process of dehydration and rehydration of GUVs containing 20 µM of CAHS12-GFP; Scale bar, 5 µm. (**H**) Quantification of IFT of droplets containing 0.1 mM of various CAHS12 constructs in mineral oil (with 0.41 mM POPC). An example of drop shape is shown for each condition. (**I**) IFT as a function of concentration for CAHS12, CAHS12 ΔC, and CAHS12 ΔN. Inset shows the morphology of a pure water droplet suspended in mineral oil containing 0.41 mM POPC. (**J**) Circularity analysis of dehydrated GUVs with increasing concentrations of different CAHS12 constructs ($n > 100$). Error bars show standard deviation.

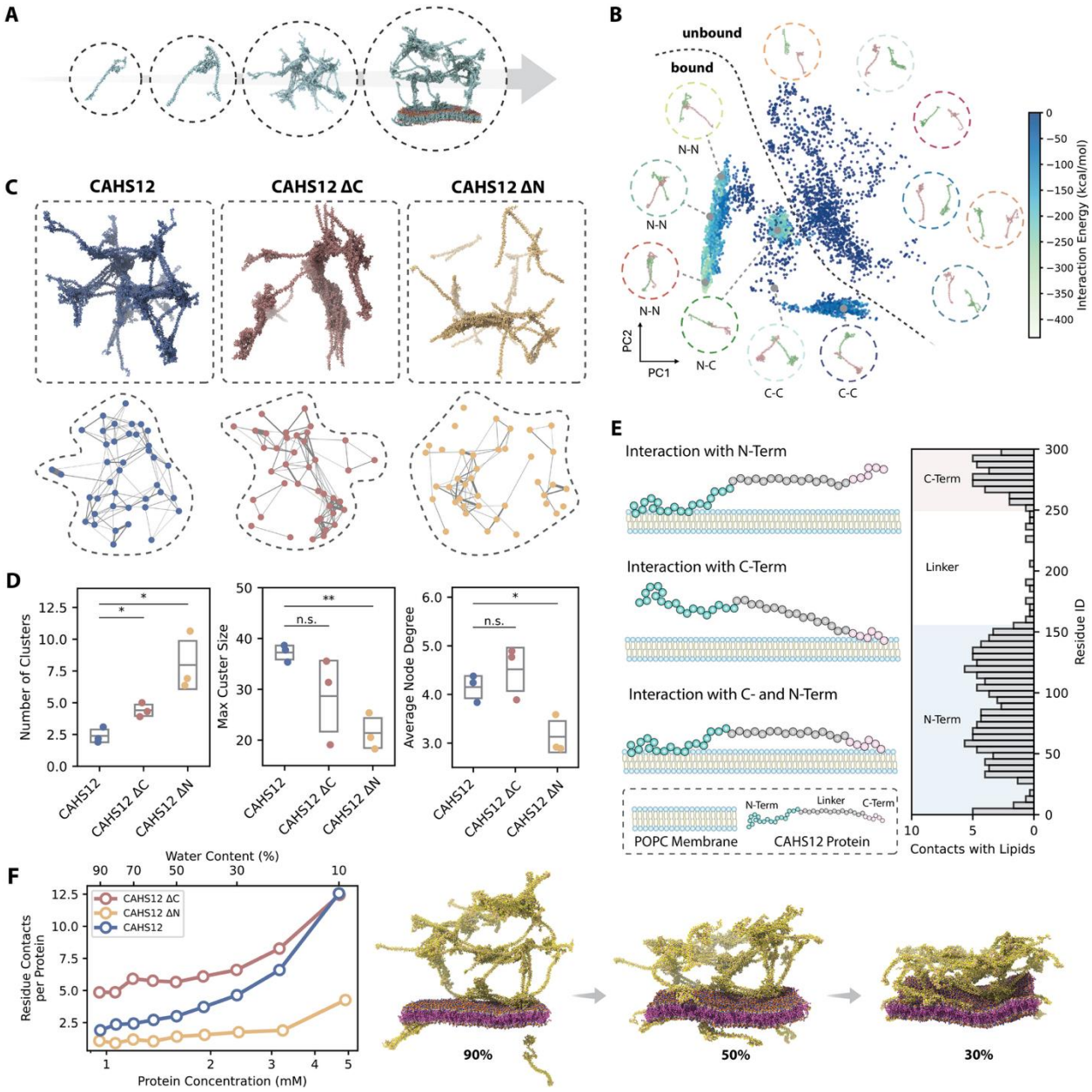

Fig. 2. Molecular dynamics simulations of CAHS12 protein assemblies and their interaction with phospholipid membranes. (**A**) Schematic depiction of the simulation systems with increasing structural complexity, ranging from a single CAHS12 monomer (left) to oligomers, fibrillar networks, and large-scale assemblies interacting with a POPC lipid membrane (right). (**B**) A PCA plot of CAHS12 dimer conformations from unbiased simulations presenting representative dimer configurations from selected clusters. The color scale indicates interaction strength based on short-range inter-protein interaction energy. (**C**) Network representations of protein assemblies for wild-type CAHS12, and the ΔC and ΔN variants. Nodes represent individual proteins; edges represent the contact among proteins; edge thickness is proportional to the inverse of the center-

of-mass distance between two proteins. (**D**) Quantification of differences in topological organization between the CAHS12, CAHS12 ΔC, and CAHS12 ΔN variants for the systems shown in (C). The number of clusters represents the count of distinct and connected protein assemblies. The maximum cluster size denotes the largest number of proteins within a single connected cluster. The average node degree indicates the mean connectivity per protein. The box bounds represent standard deviations from three independent replicates and the middle lines represent the mean. Statistical significance was assessed using Welch's t-test. (**E**) Schematic models of membrane-binding modes for the CAHS12 protein, illustrating the interaction between different domains of the protein, particularly the C- and N-terminal domains, with the POPC membrane (left). Contact frequency of residues across the whole CAHS12 sequence supporting the proposed models (right). A contact is defined as the average number of residues that are within 0.5 nm of POPC lipid headgroups. (**F**) Residue-level membrane contact analysis for CAHS12, CAHS12 ΔC, and CAHS12 ΔN during progressive water removal simulations (i.e., increasing protein concentration), along with the molecular visualization showing the CAHS12 protein and POPC membrane, mimicking the desiccation process. Contacts are defined as the number of unique residues that are within 0.5 nm of POPC lipid headgroups, normalized by the number of CAHS12 proteins. All data in (C-F) were collected from the final 500 ns of the 1500 ns simulations. Statistical analyses were performed on averaged data points from three independent simulations. A Welch's t test (two-tailed) between CASH12 and CAHS12 ΔC or CAHS12 ΔN was used in (D) to assess statistical significance. *, $p < 0.05$; **, $p < 0.01$.

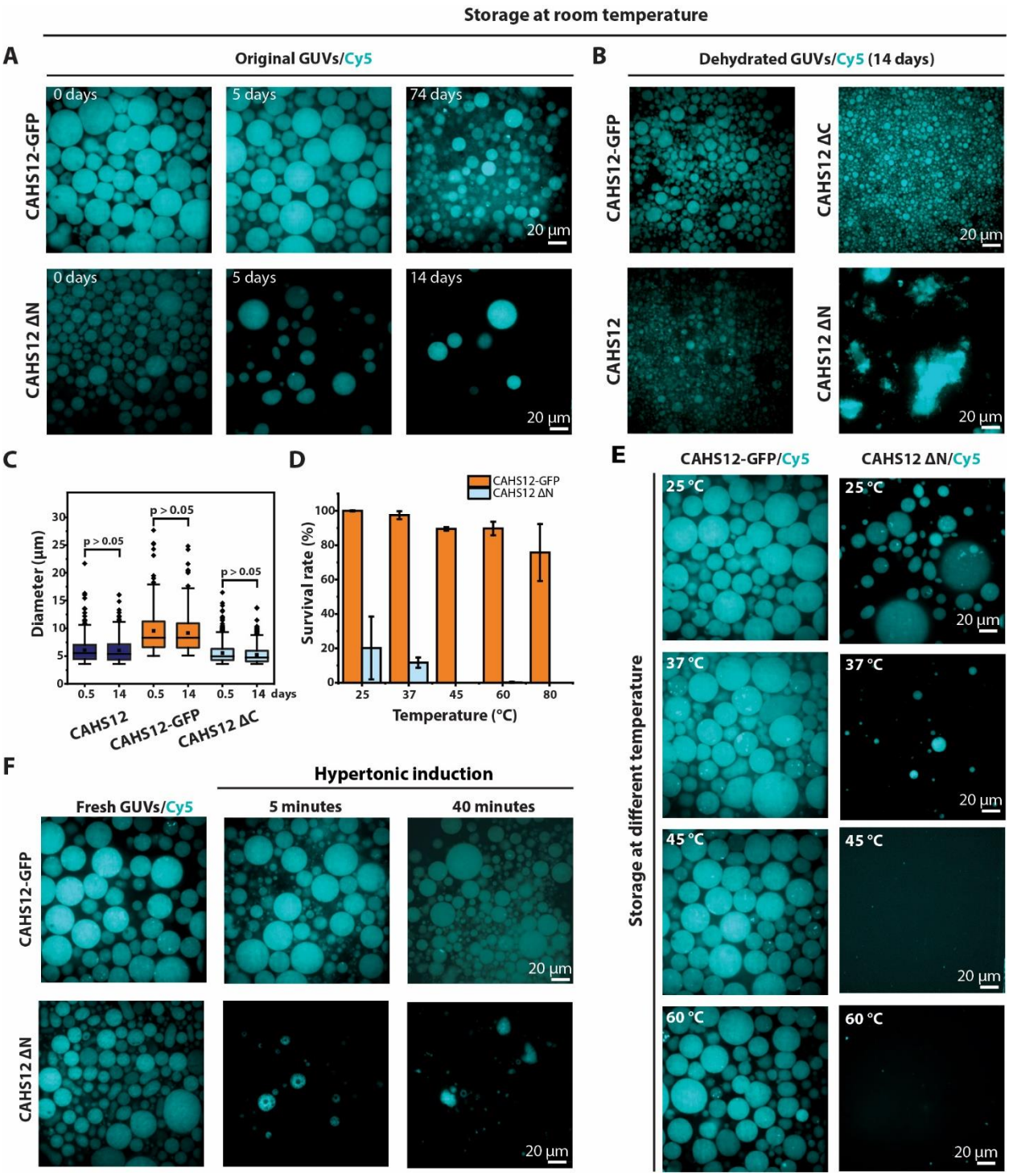

Fig. 3. CAHS12 enhances GUV stability during storage, dehydration, and osmotic stress. (**A**) Confocal images of GUVs containing Cy5 stored at room temperature. GUVs containing 280 µM CAHS12-GFP or CAHS12 ΔN were stored for 0–74 days. (**B**) Confocal images of GUVs containing 280 µM CAHS12 variant after continuous dehydration and storage for 14 days. (**C**)

Diameter distributions of GUVs containing CAHS12, CAHS12-GFP, or ΔC over continuous dehydration for 0.5 and 14 days. Survival rates (**D**) and confocal images (**E**) of GUVs after incubation at increasing temperatures (25–80 °C), where 25 °C was stored for 5 days, 37 °C and 45 °C was stored for 2 days, 60 °C was stored for 2 hours. (**F**) Fluorescence microscopy images of GUVs in an equal volume high-osmolarity glucose solution (1200 mOsm/kg) at the indicated times, where the external solution has an osmotic pressure 2.5 times that of the GUV interior. Scale bars, 20 μm.

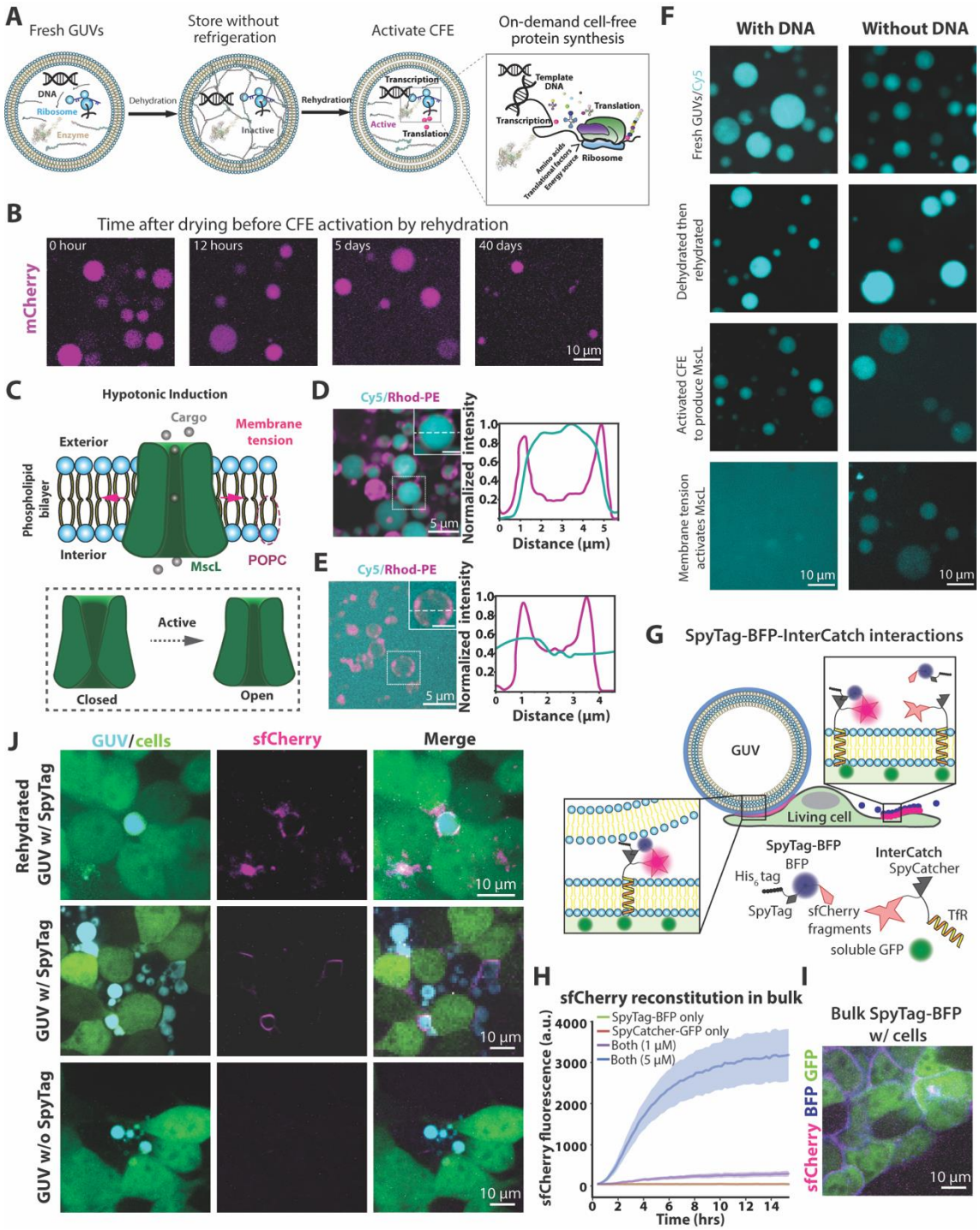

Fig. 4. Long-term preservation and activation of CFE and membrane protein function in CAHS12-stabilized GUVs. (**A**) Schematic of the workflow: synthetic components, including DNA and TX-TL machinery, are encapsulated in GUVs, dehydrated for dry storage, and rehydrated to trigger cell-free expression. (**B**) Fluorescence microscopy images of CFE activated by rehydration of dehydrated GUVs stored at room temperature for different periods (0 to 40 days). (**C**).

Schematic of MscL activation via hypotonic induction, which creates elevated membrane tension and promotes channel opening. (**D–E**) Fluorescence microscopy images and corresponding line-scan intensity profiles showing localization of Cy5 cargo and Rhod-PE membrane dye before (**D**) and after (**E**) MscL activation. Redistribution of Cy5 signal indicates membrane permeability upon functional channel activation. (**F**) Functional demonstration of MscL activity: Cy5-containing GUVs with or without DNA encoding MscL were subjected to drying, rehydration, CFE activation, and hypo-osmotic shock. Only GUVs with MscL DNA show dye leakage upon osmotic induction. **(G)** Schematic illustrating SpyTag-BFP and InterCatch-mediated interactions between synthetic cells (GUVs) and living cells, resulting in sfCherry reconstitution. SpyTag-BFP, SpyTag attached to Tag-BFP and one fragment of split sfCherry, is displayed on the GUV membrane. InterCatch, consisting of SpyCatcher fused to the complementary sfCherry fragment and the transmembrane domain of transferrin receptor (TfR), is stably expressed on HEK293T cell membranes. Soluble GFP is co-expressed for visualization. **(H)** *In vitro* sfCherry reconstitution in bulk solution using purified SpyTag-BFP and SpyCatcher-GFP. **(I)** sfCherry fluorescence is observed when InterCatch cells are incubated with purified SpyTag-BFP. **(J)** Following incubation, sfCherry reconstitution between GUV and cells is observed with both freshly prepared and dehydrated/rehydrated SpyTag-BFP GUVs. No reconstitution is seen with GUVs lacking SpyTag-BFP. All scale bars are 10 µm except for those in Fig. 4D, which are 5 µm.